minerals

MDPI

Article

Influence of Impurity Dissolution on Surface Properties and NH_3-SCR Catalytic Activity of Rare Earth Concentrate

Kai Zhang [1], Jinhao Zhu [1], Shuning Zhang [1], Na Li [1], Huijuan Luo [1], Baowei Li [2], Zengwu Zhao [2], Guang Jin [1,*] and Wenfei Wu [1,2,*]

[1] School of Energy and Environment, Inner Mongolia University of Science and Technology, Baotou 014010, China; btzk@imust.cn (K.Z.); zjhskr@163.com (J.Z.); zhangsn@163.com (S.Z.); lina@163.com (N.L.); luohuijuan1117@126.com (H.L.)

[2] State Key Laboratory of Multi-metal Resources Comprehensive Utilization, Baiyun Obo Mine, Inner Mongolia Autonomous Region, Baotou 014010, China; lbaowei@126.com (B.L.); zhaozw@imust.cn (Z.Z.)

* Correspondence: hgjg@imust.cn (G.J.); wwf@imust.edu.cn (W.W.); Tel./Fax: +86-0472-5951567 (G.J. & W.W.)

Received: 4 April 2019; Accepted: 18 April 2019; Published: 22 April 2019



Abstract: Impurity removal and modification of rare earth concentrate powder were conducted by roasting weak acid-weak alkali leaching to obtain the active components of denitrification catalysts. NH_3 selective catalytic reduction catalyst samples were prepared by mixing and kneading with pseudo-γ-Al_2O_3 boehmite as carrier. The results showed that the Ce_7O_{12} content in the active component samples increased and dispersed more evenly. The grain size of the samples was refined, the specific surface area increased, and the active sites exposed more. Ce coexists in the form of Ce^{3+} and Ce^{4+}. Fe coexists in the form of Fe^{3+} and Fe^{2+}, but Fe^{3+} is abundant. Some Ce, La, Nd, Pr, Fe, Mn, and other components formed solid melts during preparation, which increased the synergistic catalytic effect. The denitrification efficiency of the catalyst sample was 92.8% under the conditions of reaction temperature 400 °C, NO content was 600 ppm, NH_3/NO ratio was 1.5, and O_2 concentration was 4%.

Keywords: rare earth concentrate; impurity dissolution; NH_3-SCR catalyst; denitrification

1. Introduction

Rare earth metal oxides are common active catalyst components [1–3]. The low-temperature activity and anti-toxicity of transition metal oxides such as iron and manganese are hotspots in the research field of novel selective catalytic reduction (SCR) catalysts [4–9]. It has been found that composite oxides such as Cr/Zr/Ce, W/Ce, Mn/Zr/Ce, and V/Ti/Ce have good SCR catalytic effects because of their rich acidic sites and different valence states [10–13]. The addition of Ce could increase the oxygen storage capacity and surface acidity of the catalyst and promote the adsorption and activation of NH_3 on the catalyst surface [14].

Research on the preparation of catalysts from natural minerals by modification is receiving widespread attention [15,16].

The Baiyun Obo rare earth concentrate is rich in light rare earth elements such as La, Ce, Pr, and Nd (La_2O_3 26%, Ce_2O_3 50%, Nd_2O_3 16%, and Pr_2O_3 5%) and has a small amount of transition metal elements [17,18], which are necessary for many Ce-based NH_3-SCR composite oxide catalysts. However, its low-temperature catalytic activity is relatively weak, with the actual NH_3-SCR denitration rate is only 55–70% at 150–250 °C [19–21]. From the analysis of the composition-structure-property relationship of materials, natural rare earth concentrates have the material composition necessary for the preparation of rare earth metal oxide catalysts. However, because of the coexistence of various

elements and the complex embedded structure [22,23], it does not have the necessary pore structure and surface properties of catalysts. Thus, rare earth concentrates exhibit weaker catalytic properties. Surface properties and pore structure are the main factors affecting the activity of NH_3-SCR in rare earth concentrates. In this study, impurities such as SiO_2 and CaO in rare earth concentrates are regarded as the template agent in the hard template method synthesis of porous media. The liquid phase system is designed to dissolve it to form a complex pore structure. On this basis, the rare earth and transition metal oxides are exposed to the surface of the pores. Through loading of the modified rare earth concentrate onto appropriate carriers, the dispersibility, active sites, redox, and selective adsorption characteristics of the surface-active components would be enhanced. The denitration reaction activation energy and denitration reaction temperature would be lowered, thus improving the efficiency of low-temperature NH_3-SCR denitration reactions [24,25]. This effect has important theoretical significance and practical value in the research and development of new low-temperature SCR catalysts and will also provide new ideas and support for the high value-added use of Baiyun Obo rare earth concentrate.

2. Experiment

2.1. Materials

The rare earth concentrate obtained through multistage magnetic flotation separations of Bayan Obo ore was used as the raw material in the current study. The composition of the rare earth concentrate is shown in Table 1. An EDX1800E X-ray fluorescence spectrometer (Skyray Instrument Inc., Stoughton, MA, USA) was used. The test environment was a vacuum, the working voltage was 60 kV, and the working current was 60 mA. The mineral phases included mainly bastnaesite, monazite, and fluorite, and the rare earth elements were distributed among the various minerals. The chemical reagents used herein are all chemically pure.

Table 1. Elemental analysis of rare earth concentrates (unit: assemblage percentage).

Composition	Sample 1 (%)	Sample 3 (%)	Sample 4 (%)	Sample 5 (%)
Ce	24.200	23.894	24.616	31.509
O	22.600	31.319	35.596	26.298
Ca	16.500	5.162	5.434	5.612
La	12.600	12.614	10.857	15.513
Fe	7.530	7.490	7.894	10.824
Nd	7.100	4.125	3.424	5.285
P	2.190	2.400	1.643	1.478
Pr	2.070	1.921	1.544	1.401
Ba	1.490	0.219	0.201	0.159
Si	0.732	0.508	0.514	0.322
S	0.559	0.412	0.157	0.142
Mn	0.512	0.527	0.631	0.465
Zn	0.210	0.030	0.109	0.116
Ti	0.201	0.119	0.087	0.067
Gd	0.190	1.275	1.156	0.059
Th	0.166	0.043	0.034	0.037
Y	0.155	0.046	0.037	0.091
Sr	0.132	0.032	0.032	0.037
Nb	0.120	0.021	0.018	0.019
Pb	0.081	0.150	0.109	0.279
Mg	0.065	0.857	0.974	0.547
K	0.061	0.030	0.029	0.018
Al	0.029	0.158	0.119	0.101
Cu	0.015	0.011	0.013	0.009
Sm	0.454	0.427	0.431	0.361

2.2. Sample Preparation

A certain amount of rare earth concentrate was crushed, ground, sieved, dried, and then used with particle sizes of 100–200 mesh, 200–300 mesh, and 300–400 mesh. In this article, the rare earth concentrate treated with alkali ($NaHCO_3$) was calcined, acid (oxalic acid) was calcined, and then the surface properties of the modified rare earth concentrate were studied.

The modification treatment of rare earth concentrate included alkali treatment, acid treatment, and alkali–acid co-treatment. The preparation and test plan of the obtained samples are shown in Table 2. The compositions of the modified rare earth concentrates are listed in Table 1.

For preparation of Samples 3 and 4, a certain mass of sodium bicarbonate or oxalic acid was added to the beaker, and then 50 mL deionized water was added. After stirring with a magnetic agitator, a uniform solution formed at room temperature. The content of the beaker was then dried at 110 °C. It was then calcined at 500 °C for 4 h and washed with water to remove the product. The mineral material on the filter paper was dried to produce a solid sample. For sample 5, the solid sample treated with sodium hydrogen carbonate in the acid treatment process was further treated with oxalic acid to obtain a co-treated sample. Reaction equations for rare earth concentrate alkali treatment (sodium bicarbonate roasting method) are as follows:

$$2NaHCO_3 = Na_2CO_3 + H_2O + CO_2 \quad (1)$$

$$3REFCO_3 + H_2O = RE_2O_3 + REOF + 2HF + 3CO_2 \quad (2)$$

$$REFCO_3 = REOF + CO_2 \quad (3)$$

$$2REOF + Na_2CO_3 = RE_2O_3 + 2NaF + CO_2 \quad (4)$$

$$2CeFCO_3 + 1/2O_2 = Ce_2O_3F_2 + 2CO_2 \quad (5)$$

$$Ce_2O_3F_2 + Na_2CO_3 = 2CeO_2 + CO_2 + 2NaF \quad (6)$$

Reaction equations for the rare earth concentrate oxalic acid roasting method are as follows:

$$2Ca_5F(PO_4)_3 + 10C_2H_2O_4 = 10CaC_2O_4 + 6H_3PO_4 + 2HF \quad (7)$$

$$2Ca_5F(PO_4)_3 + 7C_2H_2O_4 = 7CaC_2O_4 + 3Ca(H_2PO_4)_2 + 2HF \quad (8)$$

The minerals of the fluorocarbon bismuth concentrate are basically independent, in the form of monomer particles. A small amount of fluorocarbon strontium ore forms an inclusion with lanthanum rutile or quartz, and a small amount of fluorocarbon strontium ore forms a continuous connection with quartz. Rare earth concentrates increase the specific surface area after different treatments. The increase in specific surface area of alkali roasting is caused mainly by the decomposition of minerals and the formation of cracks. The acid treatment increases the specific surface area because the surface is eroded, and voids and depressions form on the surface. The acid–base treated sample is calcined by alkali addition on the basis of acid–base corrosion; that is, erosion is formed on the surface, and the mineral is decomposed to form a crack, so that more active components are exposed on the mineral surface.

Table 2. Preparation procedure and test plan of rare earth concentrate samples.

Sample Serial Number	Raw Material	Sample Preparation			Sample	Test Methods
		Drying Temperature	Calcination Temperature	Roasting Time		
Sample 1	Concentrate	110 °C	-	-	Concentrate	XRD/TG-DSC/SEM
Sample 2	Concentrate	110 °C	500 °C	4 h	Direct roasting concentrate	XRD/BET/H_2-TPR/NH_3-TPD/NO-TPD/SEM
Sample 3	$NaHCO_3$ (4 g) + Concentrate (10 g) + H_2O (50 mL)	110 °C	500 °C	4 h	Alkali treatment concentrate	XRD/BET/H_2-TPR/NH_3-TPD/NO-TPD/SEM
Sample 4	$H_2C_2O_4$ (4 g) + Concentrate (10 g) + H_2O (50 mL)	110 °C	500 °C	4 h	Acid treated concentrate	XRD/BET/H_2-TPR/NH_3-TPD/NO-TPD
Sample 5	$NaHCO_3$ (4 g) + $H_2C_2O_4$ (4 g) + Concentrate (10 g) + H_2O (50 mL)	110 °C	500 °C	4 h	Acid-base co-processing concentrate	XRD/BET/XPS/H_2-TPR/NH_3-TPD/NO-TPD/SEM

TG-DSC: Thermogravimetric Analysis-Differential scanning calorimetry. BET: Brunauer Emmett Teller.

2.3. Analyses

2.3.1. Sample Analysis

The test equipment included an X-ray diffractometer (PANalytical B.V., Almelo, The Netherlands), Sigma-500 field emission scanning electron microscope (Zeiss, Jena, Germany), STA449C thermal analyzer (Netzsch, Oberkochen, Germany), 3H-2000PS1 automated specific surface and aperture analyzer (BeiShiDe Instrument Technology, Beijing, China), PCA-1200 temperature programmed chemical adsorption instrument (Builder, Beijing, China), VERTEX70 Fourier in-situ infrared spectrometer (Bruker, Billerica, MA, USA), and Thermo ESCALAB 250Xi X-ray photoelectron spectrometer (Thermo Fisher Scientific, Waltham, MA, USA).

2.3.2. Catalysis Activity Testing

For each test, a 1-g sample was placed on the reaction bed. The composition of the flue gas was monitored by the DX4000 type Fourier infrared spectrum flue gas analyzer (Gasmet, Helsinki, Finland).

The testing instrument consisted of a vertical reaction tube furnace, Fourier infrared spectrum flue gas analyzer, and computer data acquisition system, with available online measurement of flue gas composition. A reaction bed was used to support the catalyst. The experimental principle of its activity is:

$$4NO + 4NH_3 + O_2 = 4N_2 + 6H_2O \quad (9)$$

$$2NO_2 + 4NH_3 + O_2 = 3N_2 + 6H_2O \quad (10)$$

$$6NO + 4NH_3 = 5N_2 + 6H_2O \quad (11)$$

$$6NO_2 + 8NH_3 = 7N_2 + 12H_2O \quad (12)$$

For each test, a 1-g sample was placed on the heated reaction bed in the quartz tube. After testing, the furnace was heated at 10 °C/min to the reaction temperature, and the reaction gases bubbled for 30 min until the test temperature and the gas concentration became stable. The denitration efficiency of the catalyst was calculated according to Formula (13):

$$\eta = \frac{(NO)_{\text{in}} - (NO)_{\text{out}}}{(NO)_{\text{out}}} \times 100\% \quad (13)$$

where $(NO)_{\text{in}}$ is the initial *NO* concentration and $(NO)_{\text{out}}$ is the *NO* concentration during the catalysis reaction at different reaction temperatures.

3. Results and Discussion

3.1. Characterization and Thermogravimetric Analysis of Rare Earth Concentrate

It can be seen in Table 1 that although the Baotou rare earth concentrate has a high content of rare earth elements, there are many non-rare earth impurities and complex components. Our research group has performed thermogravimetric (TG) analysis (Figure 1) and X-ray powder diffraction (XRD) analysis (Figures 2 and 3) of the raw rare earth concentrate and XRD analysis of rare earth ore concentrate after modification and calcination. From the XRD characterizations, the presence states of the main elements and the ore phase structures can be observed.

Figure 1 shows the TG differential scanning calorimetry (DSC) curve of the rare earth concentrate. Because of the nearly complete desorption of adsorbed gas, the TG curve remained stable up to 400 °C. Within the range of 400–550 °C, a broad endothermic peak appears, with obvious weight loss. It is attributed to thermal decomposition of the rare earth concentrate. Within the range of 550–850 °C, the TG curve remained stable, indicating that the ore material itself was in an endothermic state. Within the range of 850–1000 °C, the TG curve shows continuous weight loss, with a broad endothermic peak

in the DSC curve. This may be attributed to the decomposition of carbonate materials during roasting and local melting caused by sintering.

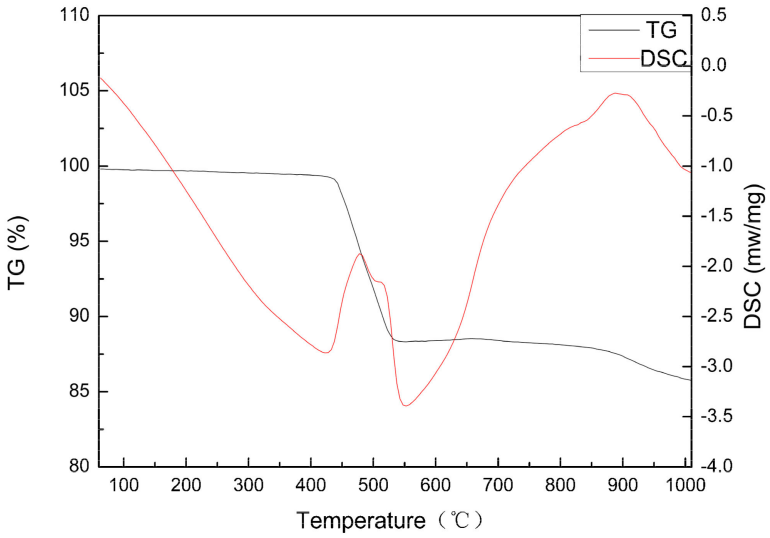


Figure 1. TG curve of the rare earth concentrate.

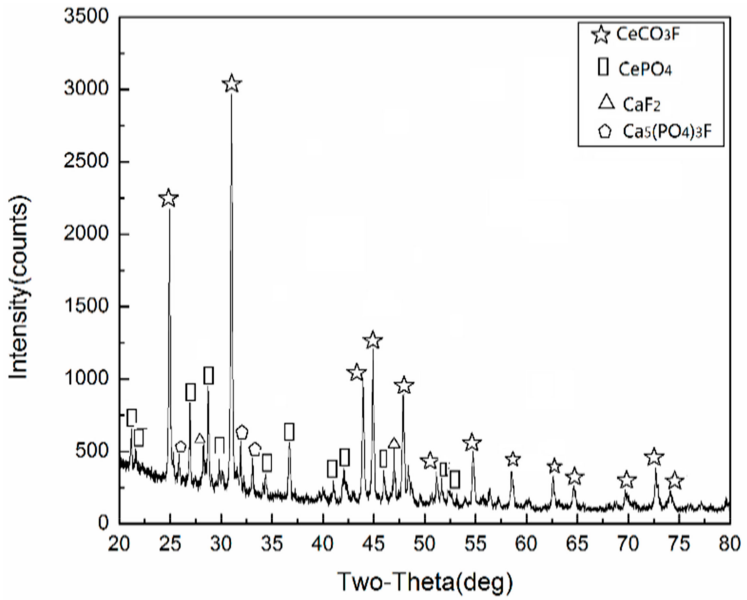


Figure 2. XRD pattern of the rare earth concentrate.

As shown in Figures 2 and 3, the main components of the rare earth concentrate are bastnaesite and monazite. For the alkali-treated rare earth concentrate, a new material (NaF) formed. Compared with direct roasted rare earth concentrate, the increase in peak intensity of the Ce_7O_{12} phase indicates that the addition of alkali could promote the conversion of more bastnaesite to Ce_7O_{12}. Further washing could remove NaF and residual Na_2CO_3 produced during defluorination and improve the purity of Ce_7O_{12}. After further treatment with oxalic acid, the peak height of the Ce_7O_{12} crystal phase decreases and the peak width becomes larger. Meanwhile, the peak of the calcium fluorophosphate crystal phase disappears. The combined modification of sodium bicarbonate and oxalic acid is expected to improve the defluorination efficiency and reduce impurities and to increase the content and dispersion of Ce_7O_{12}. The active component is exposed while increasing the acidity level, effectively increasing the activity of the catalyst. $CePO_4$ was stable during modification of the mineral materials, and no significant changes appeared in each treatment.

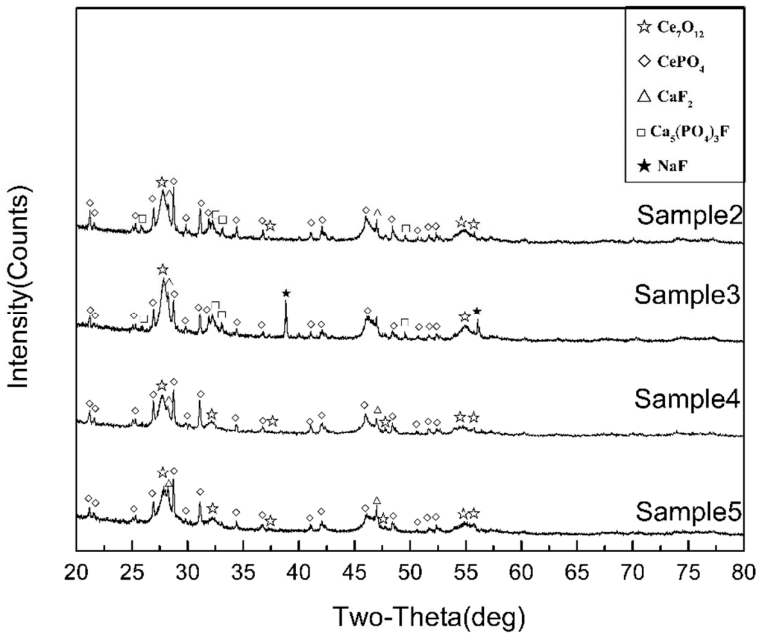


Figure 3. XRD patterns of the modified rare earth concentrates after calcination.

3.2. Catalytic Activity of Rare Earth Concentrate

While the reaction temperature was stable at 400 °C, no change in the NO content occurred for 12 min, and then the NO content began to decrease, approaching a steady state at 42 min. The NH_3-SCR performance of the Baiyun Obo rare earth concentrate was tested by the denitrification performance test, which indicated that the unprocessed Baiyun Obo rare earth concentrate had obvious catalytic performance in the SCR denitrification reaction. The denitrification rate increased with the decrease in particle size of the original ore (Figure 4), because the smaller the particle size, the higher its relative dispersion, and the larger the contact area between the active components and NH_3 and NO. Therefore, under the catalysis of rare earth ore, the activation energy of NH_3 and NO reaction decreases, the frequency factor increases, the reduction capacity of NH_3 to NO increases, and the reaction is further promoted. Therefore, a rare earth concentrate with a particle size less than 300 mesh was used in the experiment.

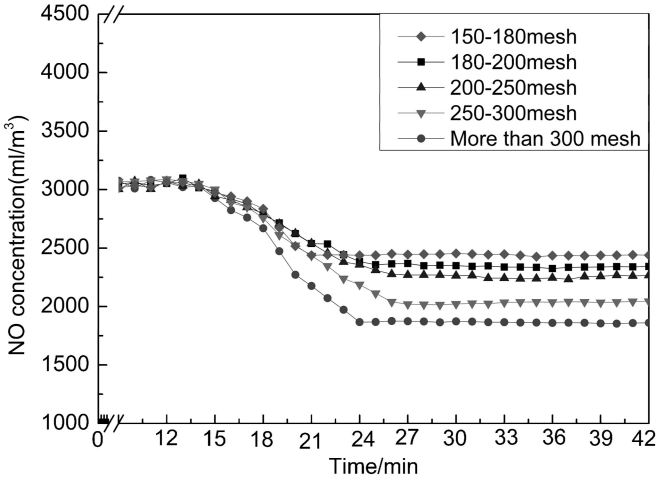


Figure 4. Relationship between the particle size and denitrification rate of primary ore.

3.3. Activity Test for Different Treatments of Concentrate

As shown in Figure 5, the activity of the overall catalyst increased from 300 °C to 500 °C and decreased slightly after 500 °C. The catalytic activity of the sample after the acid and alkali co-treatment was greatly increased with respect to the sample after direct calcination. The treated sample temperature window and catalytic activity greatly increased at the same time. The specific surface area of element contact during catalytic activity increased by Ce, Fe, and other elements, and calcination was performed so that the effective element is exposed on the surface of the mineral material to form a solid solution, thereby increasing catalytic activity.

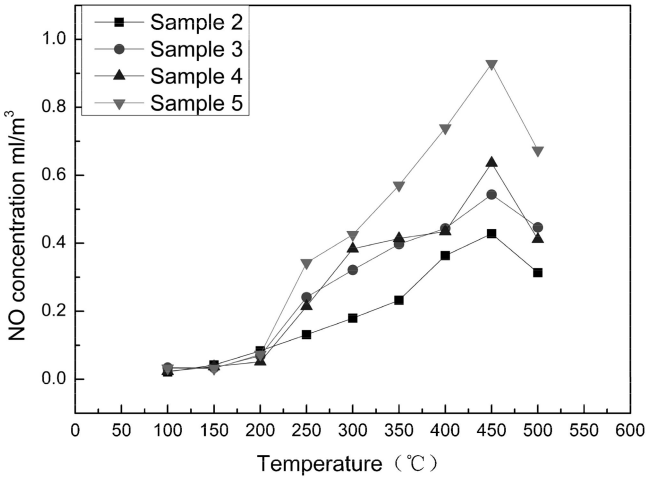


Figure 5. Activity test for different treatments of concentrate.

3.4. Properties and Micromorphology of Modified Rare Earth Concentrates

Because Ce in the rare earth concentrate occurs mainly in the form of $CeFCO_3$, which is relatively inert to chemical catalysis, the catalytic activity of Ce is largely inhibited, and the catalytic activity of the rare earth concentrate at low temperature is weak. Therefore, removing and modifying the rare earth concentrates, thus increasing the content of active substances, could provide a material basis to optimize catalytic performance.

3.4.1. Properties of Modified Rare Earth Concentrates

Surface Properties

After the rare earth concentrate was calcined under different conditions, its physical properties were tested. The Brunauer-Emmett-Teller results are shown in Table 3.

Table 3. Physical properties of the modified rare earth concentrates.

Physical Properties	Sample 2	Sample 3	Sample 4	Sample 5
Specific surface area (m^2/g)	154.9	190.5	212.4	208.0
Pore volume (mL/g)	0.4	0.4	0.57	0.6
Average aperture (nm)	12.7	11.9	10.1	10.7

It can be seen in Table 3 that the maximum surface area of the rare earth concentrate could be increased to 212.353 m^2/g after treatment, which promotes a more uniform distribution of the active components. This could facilitate full contact of the reaction gas with the surface-active adsorption sites of the catalyst, thus increasing the adsorption amount and promoting the SCR reaction. The pore volume was increased to 0.57 mL/g, the average pore size was reduced, and the micropores were reduced to 10.10 nm, forming a larger pore volume and a richer medium pore structure. This will

provide more active adsorption sites for reaction gas and facilitate the timely desorption and discharge of reaction products in the pores, thereby promoting an efficient SCR reaction.

Valences of Ce and Fe Elements

Surface X-ray photoelectron spectroscopy (XPS) analysis of Ce and Fe was performed for sample 5. As shown in Figure 6, the XPS spectrum of the Ce 3d orbital of modified rare earth concentrate sample 5 is complex, showing three peak groups. The two types of Ce 3d 3/2 and Ce 3d 5/2 peaks are labeled with v and u, respectively, where v_0, v_1, v_2, and v_3 represent the electron binding energy peaks of Ce 3d 3/2 and u_0, u_1, u_2, and u_3 represent the electron binding energy peaks of Ce 3d 5/2. The peaks of v_0, v_2, v_3, u_0, u_2, and u_3 correspond to the characteristic peaks of Ce^{4+}, and the two peaks of v_1 and u_1 correspond to the characteristic peaks of Ce^{3+} [26]. It is revealed that the catalyst has a certain number of Ce^{4+}/Ce^{3+} redox electron pairs, which promote the storage and release of surface oxygen, increase surface oxidation, and increase transformation of NO to NO_2 at the active site.

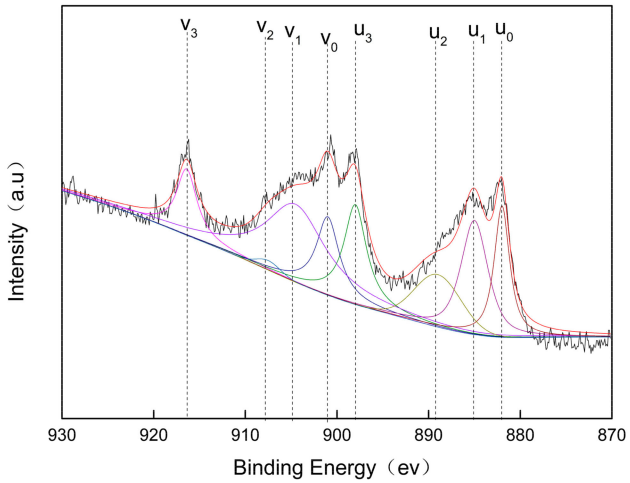


Figure 6. XPS spectrum of the Ce 3d orbital.

The XPS spectrum of the Fe 2p orbital on the surface of modified rare earth concentrate Sample 5 (Figure 7) showed two strong peaks and one weak auxiliary peak. The two strong peaks correspond to Fe 2p 3/2 (the binding energy is 711 eV) and Fe 2p 1/2 (the binding energy is ~725 eV). According to the standard spectrum of Fe 2p, the two peaks correspond to the characteristic peaks of Fe^{3+}. The auxiliary peak in the range of 718–721 eV represents the characteristics of Fe^{2+}. The XPS results indicate that Fe coexists in the form of Fe^{2+} and Fe^{3+}, and Fe^{3+} dominates [27].

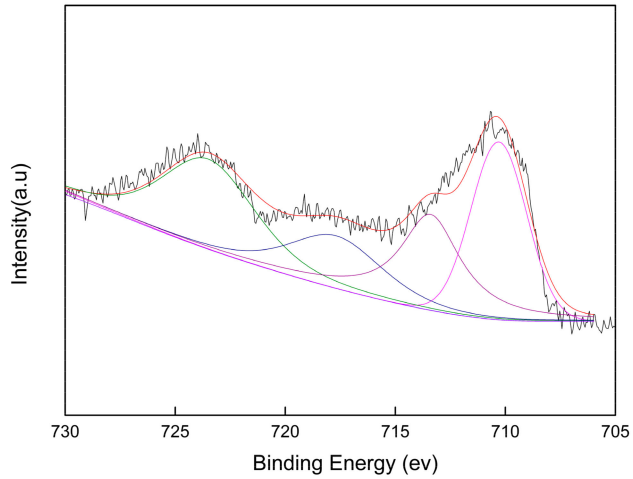


Figure 7. XPS spectrum of the Fe 2p orbital on the surface of the modified rare earth concentrate.

Surface Reduction Ability Characterization

To investigate the ability of metal ions to reduce to low-valent metal ions and to absorb and release oxygen, H_2 temperature-programmed reduction (TPR) experiments were carried out. The results are shown in Figure 8.

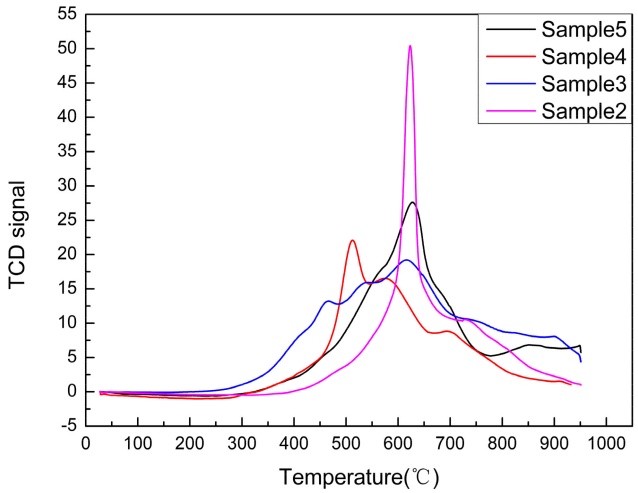


Figure 8. H_2-TPR (temperature-programmed reduction) diagram of modified rare earth concentrate.

It can be seen in Figure 8 that after direct roasting of the rare earth concentrate, there is a peak at 620 °C and a shoulder peak at 740 °C. After alkali modification treatment, there were multiple reduction peaks in the wide temperature range of 300–900 °C. After alkali–acid co-modification treatment, there were multiple reduction peaks in the wide temperature range of 400–800 °C. The main peak was at 620 °C, the two shoulder peaks are at 550 °C and 650 °C, and a weak broad peak was above 800 °C. Compared with the direct calcined sample, the temperature domain of the reduction peak was broadened, and the peak was moved toward the low-temperature region. The peak area of Sample 3 was 3087.3, the peak area of sample 4 was 4665.5, and the peak area of Sample 5 was 4032.2. The peak area of modified rare earth concentrates was larger than that of the unmodified one, indicating that the modification treatment could increase the oxygen storage capacity and redox ability of the catalyst.

Surface Acidity Characterization

To investigate whether the modification treatment would affect the surface acidity of rare earth concentrates, NH_3 temperature-programmed desorption (TPD) experiments were carried out on three kinds of rare earth concentrates with different modification treatments. The test results are shown in Figure 9.

It can be seen in Figure 9 that the order of surface acid amounts is acid–alkali co-treatment (NH_3 desorption amount 1272.62 μmol/g) > acid treatment (984.79 μmol/g) > alkali treatment (778.20 μmol/g) > direct calcination treatment (642.06 μmol/g). Four samples showed a weak desorption peak in the low temperature range (100–250 °C). This finding shows that many substances work together to make a large amount of NH_3 adsorb on the surface of the catalyst, increase the amount of surface acid, and increase the number of surface active sites, which indicates that the surfaces of particles can be modified after acid–base roasting treatment.

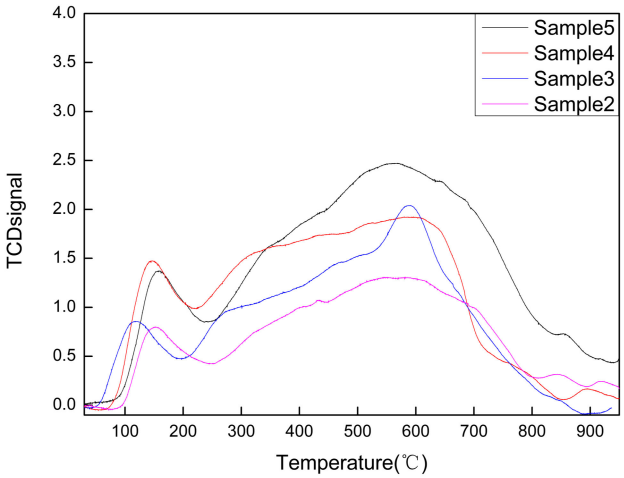


Figure 9. NH_3-TPD diagram of modified rare earth concentrate.

Characterization of Adsorption Capacity of NO

The adsorption capacity of modified rare earth concentrates for NO was investigated in a NO temperature-programmed adsorption–desorption experiment. The results are shown in Figure 10.

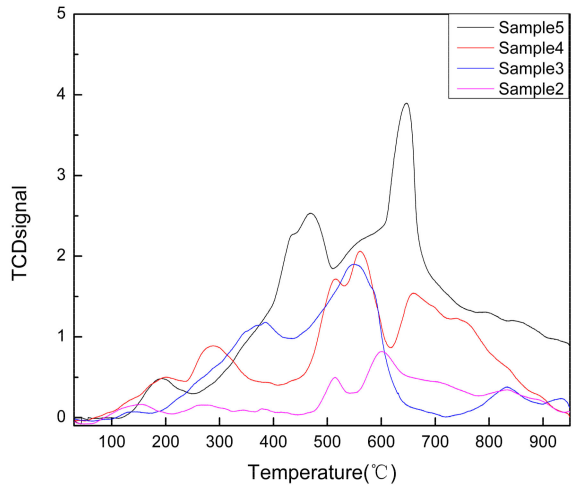


Figure 10. NO-TPD curve of modified rare earth concentrate.

In the curves shown in Figure 10, compared with direct baking, the NO adsorption effect of rare earth concentrates after alkali treatment, acid treatment, and alkali–acid co-treatment was significantly increased. Compared with the direct roasted sample, the desorption peak of the alkali-treated sample was increased and shifted toward the low temperature range. The desorption peak of the acid-treated sample was obviously improved. After alkali–acid co-treatment, the adsorption capability was significantly increased throughout the temperature range. The acid–base co-processed sample has a greater specific surface area relative to the acid- or base-treated samples, providing more adsorption sites for NO. This is an important factor in the reaction efficiency of NO conversion.

3.4.2. Microscopic Appearance of the Modified Rare Earth Concentrate

Scanning electron microscope (SEM) images of the modified rare earth concentrate are shown in Figure 11.

As shown in the SEM images (Figure 11a,b), after direct roasting the surfaces of the minerals changed from smooth to folded, and cracks appeared. After alkali modification, there were many uneven corrosion marks on the surface of the ore. After acid modification, the original structure of the

ore collapsed and broke, and the powder was refined. After the alkali–acid co-modification treatment, a lot of debris appeared on the surface of the ore, there were many pore structures, and the specific surface area increased significantly. Through SEM mapping analysis, it can be seen that Ce, La, Nd, Fe, and other active metal elements existed in the active components after the catalyst formed. The Ce_7O_{12} particles were found in selected large particles. Energy-dispersive X-ray spectroscopy (EDS) mapping showed that the La, Nd, and Pr rare earth elements that originated from $CeFCO_3$ were uniformly distributed in Ce_7O_{12}, forming a solid solution (Figure 12).

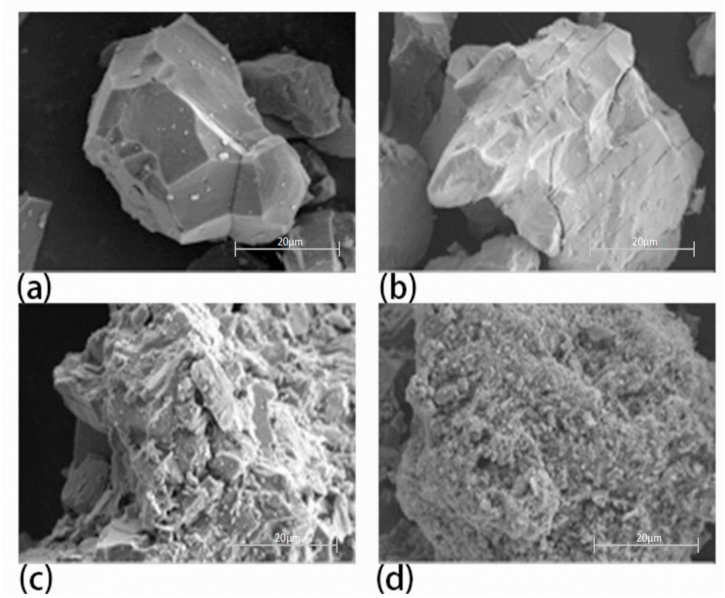


Figure 11. SEM images of rare earth concentrate: (**a**) sample 1, (**b**) sample 2, (**c**) sample 3, and (**d**) sample 4.

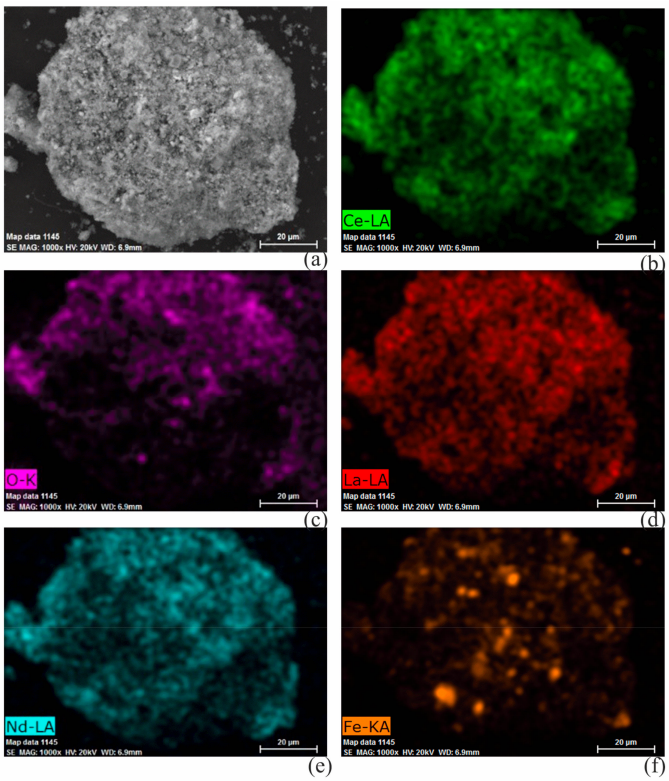


Figure 12. EDS mapping of Ce_7O_{12} particles: (**a**) SEM image, (**b**) Ce, (**c**) O, (**d**) La, (**e**) Nd, and (**f**) Fe.

4. Conclusions

The dissolution of impurities (Ca, Si) has an important effect on the surface properties of pores and can increase redox of the surface of rare earth concentrates and the adsorption properties of NH_3 and NO. After impurity removal treatment, the Ce_7O_{12} content of Baiyun Obo rare earth concentrate increased and the dispersion was more uniform, the specific surface area increased, the average pore diameter decreased, and the pore volume increased. Some Ce, La, Nd, Pr, Fe, Mn, and other components formed solid melts during preparation, which increased the synergistic catalytic effect. Ce coexists in the form of Ce^{3+} and Ce^{4+}. Fe coexists in the form of Fe^{3+} and Fe^{2+}, but Fe^{3+} is abundant. Denitrification efficiency of the catalyst sample was 92.8% under the conditions of reaction temperature 400 °C, NO content was 600 ppm, NH_3/NO ratio was 1.5, and O_2 concentration was 4%.

Author Contributions: Conceptualization, K.Z.; Investigation, S.Z.; Project administration, N.L. and H.L.; Validation, B.L. and Z.Z.; Writing–original draft, J.Z.; Writing–review & editing, W.W. and G.J.

Funding: The investigation was financially supported by the National Natural Science Foundation of China (51866013) and by the Natural Science Foundation of the Inner Mongolia Autonomous Region (2018MS02013).

Conflicts of Interest: The authors declare no conflict of interest.

References

1. Shi, Z.; Yang, X.; Yan, S. Photocatalytic activity of cerium-doped mesoporous TiO_2 coated Fe_3O_4 magnetic composite under UV and visible light. *J. Rare Earths* **2012**, *30*, 355–360. [CrossRef]
2. Al-Musa, A.; Al-Saleh, M.; Ioakeimidis, Z.C.; Ouzounidou, M.; Yentekakis, I.V.; Konsolakis, M.; Marnellos, G.E. Hydrogen production by iso-octane steam reforming over Cu catalysts supported on rare earth oxides (REOs). *Int. J. Hydrogen Energy* **2014**, *39*, 1350–1363. [CrossRef]
3. Thirupathi, B.; Smirniotis, P.G. Co-doping a metal (Cr, Fe, Co, Ni, Cu, Zn, Ce, and Zr) on Mn/TiO_2 catalyst and its effect on the selective reduction of NO with NH_3 at low-temperatures. *Appl. Catal. B Environ.* **2011**, *110*, 195–206. [CrossRef]
4. Kim, Y.J.; Kwon, H.J.; Heo, I.; Nam, I.-S.; Cho, B.K.; Choung, J.W.; Cha, M.-S.; Yeo, G.K. Mn–Fe/ZSM5 as a low-temperature SCR catalyst to remove NO*x* from diesel engine exhaust. *Appl. Catal. B Environ.* **2012**, *126*, 9–21. [CrossRef]
5. Yang, S.; Qi, F.; Xiong, S.; Dang, H.; Liao, Y.; Keung, W.; Li, J. MnO_X supported on Fe–Ti spinel: A novel Mn based low temperature SCR catalyst with a high N_2 selectivity. *Appl. Catal. B Environ.* **2016**, *181*, 570–580. [CrossRef]
6. Casanova, M.; Schermanz, K.; Llorca, J.; Trovarelli, A. Improved high temperature stability of NH_3-SCR catalysts based on rare earth vanadates supported on TiO_2–WO_3–SiO_2. *Catal. Today* **2012**, *184*, 227–236. [CrossRef]
7. Wei, Y.; Chen, Y.; Wang, R. Rare earth salt of 12-tungstophosphoric acid supported on iron oxide as a catalyst for selective catalytic reduction of NO_X. *Fuel Process. Technol.* **2018**, *178*, 262–270. [CrossRef]
8. Zhao, K.; Meng, J.; Lu, J.; He, Y.; Huang, H.; Tang, Z.; Zhen, X. Sol-gel one-pot synthesis of efficient and environmentally friendly iron-based catalysts for NH_3-SCR. *Appl. Surf. Sci.* **2018**, *445*, 454–461. [CrossRef]
9. Shi, A.; Wang, X.; Yu, T.; Shen, M. The effect of zirconia additive on the activity and structure stability of V_2O_5/WO_3–TiO_2 ammonia SCR catalysts. *Appl. Catal. B Environ.* **2011**, *106*, 359–369. [CrossRef]
10. Vuong, T.H.; Radnik, J.; Rabeah, J.; Bentrup, U.; Scheneider, M.; Atia, H.; Armbruster, U.; Grunert, W.; Bruckner, A. Efficient VO_X/Ce–$_X$Ti$_X$O$_2$ Catalysts for Low-Temperature NH_3-SCR: Reaction Mechanism and Active Sites Assessed by in Situ/Operando Spectroscopy. *Acs Catal.* **2017**, *7*, 1693–1705. [CrossRef]
11. Zhou, C.; Zhang, Y.; Wang, X.; Xu, H.; Sun, K.; Shen, K. Influence of the addition of transition metals (Cr, Zr, Mo) on the properties of MnO_X–FeO_X catalysts for low-temperature selective catalytic reduction of NO_X by Ammonia. *J. Colloid. Interface Sci.* **2013**, *392*, 319–324. [CrossRef]
12. Yue, B.; Zhou, R.; Wang, Y.; Zheng, X. Influence of transition metals (Cr, Mn, Fe, Co and Ni) on the methane combustion over Pd/Ce–Zr/Al_2O_3 catalyst. *Appl. Surf. Sci.* **2006**, *252*, 5820–5828. [CrossRef]
13. Fernandez-Garcia, M.; Martinez-Arias, A.; Iglesias-Juez, A.; Hungria, A.B.; Anderson, J.A.; Conesa, J.C.; Soria, J. Behavior of bimetallic Pd/Cr/Al_2O_3 and Pd/Cr/(Ce,Zr)O_X/Al_2O_3 catalysts for CO and NO elimination. *J. Catal.* **2003**, *214*, 220–233. [CrossRef]

14. He, H.; Dai, H.X.; Au, C.T. Defective structure, oxygen mobility, oxygen storage capacity, and redox properties of RE-based (RE = Ce, Pr) solid solutions. *Catal. Today* **2004**, *90*, 245–254. [CrossRef]
15. Tran, U.P.N.; Le, K.K.A.; Phan, N.T.S. Expanding Applications of Metal−Organic Frameworks: Zeolite Imidazolate Framework ZIF-8 as an Efficient Heterogeneous Catalyst for the Knoevenagel Reaction. *ACS Catal.* **2011**, *1*, 120–127. [CrossRef]
16. Lan, X.; Gao, J.; Du, Y.; Guo, Z. Mineral evolution and separation of rare-earth phases from Bayan Obo rare-earth concentrate in a super-gravity field. *J. Alloy. Compd.* **2018**, *731*, 873–880. [CrossRef]
17. Wang, L.; Liang, T.; Zhang, Q.; Li, K. Rare earth element components in atmospheric particulates in the Bayan Obo mine region. *Environ. Res.* **2014**, *131*, 64–70. [CrossRef]
18. Xu, C.; Campbell, L.H.; Kynicky, J.; Allen, C.M.; Chen, Y.; Huang, Z.; Qi, L. Comparison of the Daluxiang and Maoniuping carbonatitic REE deposits with Bayan Obo REE deposit, China. *Lithos* **2008**, *106*, 12–24. [CrossRef]
19. Wu, Z.; Jiang, B.; Liu, Y. Effect of transition metals addition on the catalyst of manganese/titania for low-temperature selective catalytic reduction of nitric oxide with ammonia. *Appl. Catal. B Environ.* **2008**, *79*, 347–355. [CrossRef]
20. Gao, G.; Shi, J.-W.; Liu, C.; Cao, C.; Fan, Z.; Niu, C. Mn/CeO_2 catalysts for SCR of NO_X with NH_3: Comparative study on the effect of supports on low-temperature catalytic activity. *Appl. Surf. Sci.* **2017**, *411*, 338–346. [CrossRef]
21. Yang, J.; Ma, H.; Yanamoto, Y.; Yu, J.; Xu, G.; Zhang, Z.; Suzuki, Y. SCR catalyst coated on low-cost monolith support for flue gas denitration of industrial furnaces. *Chem. Eng. J.* **2013**, *230*, 513–521. [CrossRef]
22. Yao, X.; Kong, T.; Yu, S.; Li, L.; Yang, F.; Dong, L. Influence of different supports on the physicochemical properties and denitration performance of the supported Mn-based catalysts for NH_3-SCR at low temperature. *Appl. Surf. Sci.* **2017**, *402*, 208–217. [CrossRef]
23. Xu, C.; Liu, J.; Zhao, Z.; Yu, F.; Cheng, K.; Wei, Y.; Duan, A.; Jiang, G. NH_3-SCR denitration catalyst performance over vanadium-titanium with the addition of Ce and Sb. *J. Environ. Sci.* **2015**, *31*, 74–80. [CrossRef]
24. Jiang, B.; Li, Z.; Lee, S.-C. Mechanism study of the promotional effect of O_2 on low-temperature SCR reaction on Fe–Mn/TiO_2 by DRIFT. *Chem. Eng. J.* **2013**, *225*, 52–58. [CrossRef]
25. Klukowski, D.; Ballea, P.; Geigera, B.; Wagloehnera, S.; Kuretia, S.; Kimmerleb, B.; Baikerb, A.; Grunwaldtc, J.-D. On the mechanism of the SCR reaction on Fe/HBEA zeolite. *Appl. Catal. B Environ.* **2009**, *93*, 185–193. [CrossRef]
26. Priolkar, K.R.; Parthasarathi Bera, P.R.; Sarode, M.S.; Hegde, S.; Emura, S.; Kumashiro, R.; Lalla, N. Formation of $Ce_{1-x}Pd_xO_{2-\delta}$ solid solution in combustion-synthesized Pd/CeO_2 catalyst: XRD, XPS, and EXAFS investigation. *Chem. Mater.* **2002**, *14*, 2120–2128. [CrossRef]
27. Yamashita, T.; Hayes, P. Analysis of XPS spectra of Fe^{2+} and Fe^{3+} ions in oxide materials. *Appl. Surf. Sci.* **2008**, *254*, 2441–2449. [CrossRef]



© 2019 by the authors. Licensee MDPI, Basel, Switzerland. This article is an open access article distributed under the terms and conditions of the Creative Commons Attribution (CC BY) license (http://creativecommons.org/licenses/by/4.0/).